The Mu3e Experiment

Gavin Hesketh,[1] **Sean Hughes,**[2] **Ann-Kathrin Perrevoort,**[3] **and Nikolaos Rompotis**[2] **on behalf of the Mu3e Collaboration**

[1]*University College London*

[2]*University of Liverpool*

[3]*Karlsruhe Institute of Technology*

E-mail: gavin.hesketh@ucl.ac.uk

ABSTRACT:

The Mu3e experiment at the Paul Scherrer Institut will search for the lepton-number-violating decay $\mu^+ \to e^+e^-e^+$, extending the sensitivity by four orders of magnitude compared to existing limits. This probe of new physics is complementary to the existing collider, dark matter and neutrino particle physics programmes, and part of a global programme investigating the charged lepton flavour sector. As well as the main $\mu^+ \to e^+e^-e^+$ search, Mu3e will also extend the sensitivity to low-mass dark photons, and additional flavour-violating decays involving long-lived or stable particles.

Contents

1 Introduction

Charged lepton flavour violating (CLFV) processes offer unique discovery potential for physics beyond the Standard Model (BSM), bringing sensitivity to new physics that is complementary to the existing collider, dark matter and neutrino particle physics programmes. The Mu3e experiment [1] at the Paul Scherrer Institut (PSI) is part of a global programme of experiments searching for the "golden channels" of CLFV in the muon sector: $\mu^+ \to e^+\gamma$, $\mu^+ \to e^+e^-e^+$, $\mu^-N \to e^-N$. This programme will bring a significant increase in sensitivity compared to previous searches, probing new physics mass scales up to 10^3 - 10^4 TeV. Of the experiments which will start taking data in the coming years, Mu3e is the only one which will search for the decay $\mu^+ \to e^+e^-e^+$ (MEG-II [2, 3] targets the $\mu^+ \to e^+\gamma$ signal, while Mu2e [4], COMET [5] and DeeMe [6] will search for $\mu^-N \to e^-N$).

Flavour violation is a known feature of the quark and neutrino sectors of the Standard Model. And while charged lepton flavour appears to be conserved, it is not protected by any known global symmetry and occurs at the 1-loop level via neutrino oscillation. In the Standard Model, it is suppressed to an unobservably small rate $\mathcal{O}(10^{-50})$ [7, 8] by factors of $\left(\Delta m_{ij}^2/m_W^2\right)^2$ in those loops, where Δm_{ij} is the squared mass difference between the neutrino mass eigenstates i and j. However, significant enhancements to this rate are predicted by many BSM scenarios, and the observation of any CLFV signal would be the unambiguous observation of new physics.

The nature of any CLFV signal will depend on the underlying physics. For example, in processes dominated by γ-penguin diagrams, the $\mu^+ \to e^+\gamma$ rate is expected to be higher than $\mu^+ \to e^+e^-e^+$ or $\mu^-N \to e^-N$. However, the reverse is true if Z or H-penguin diagrams or tree level Z' or lepto-quark models dominate. There is an extensive and growing literature exploring these different scenarios, for example [9], which can be parameterised with a general effective operator approach, as used in Section 2. However, the conclusion is clear: exploring all three "golden" muon channels is essential.

The current best limit on $\mu^+ \to e^+e^-e^+$ was set by the SINDRUM collaboration [10], excluding a branching ratio over 1.0×10^{-12} at 90% confidence level (CL). With a two-phase approach, Mu3e aims to extend the sensitivity to 10^{-16}. Phase-1, currently under construction, will utilise the πE5 beam-line at PSI to study up to 10^8 muon (μ^+) stops per second and reach a sensitivity of 2×10^{-15} on the branching fraction. An upgraded detector for Phase-2 plans to make use of the High-Intensity Muon Beam upgrades at PSI to study 2×10^9 muon stops per second and reach the target sensitivity of 10^{-16} on the branching fraction.

Mu3e uses an innovative detector design, with extremely low material budgets in order to minimise multiple scattering for low energy electrons. It consists of four layers of HV-MAPS silicon pixel sensors thinned to 50 μm, and scintillating fibre and tile detectors providing sub-ns timing resolution. The detector is surrounded by a solenoid magnet providing a 1 T field; electrons from muon decays can pass through the detector several times as they follow helical paths in this field. This significantly extends the lever-arm for measurement, and hence the momentum resolution.

As well as the main $\mu^+ \to e^+e^-e^+$ search, Mu3e can search for signatures of the

form $\mu^+ \to e^+ X$, where X can decay to $e^+ e^-$ promptly, after travelling some distance, or escaping the detector before decaying. This covers a range of ALP, familon, majoron and Z' models.

This White-paper will briefly cover the expected sensitivity of the various searches possible at Mu3e, along with an overview of the experimental design.

2 The search for $\mu^+ \to e^+ e^- e^+$

To study the effects of different BSM scenarios on the decay kinematics, and therefore detector acceptance, we will consider the general effective Lagrangian proposed by Kuno and Okada [11]:

$$
\begin{aligned}
\mathcal{L}_{\mu \to eee} = -\frac{4G_F}{\sqrt{2}} \Big[& m_\mu A_R \, \overline{\mu_R} \sigma^{\mu\nu} e_L F_{\mu\nu} + m_\mu A_L \, \overline{\mu_L} \sigma^{\mu\nu} e_R F_{\mu\nu} \\
& + \ g_1 \, (\overline{\mu_R} e_L) \, (\overline{e_R} e_L) + g_2 \, (\overline{\mu_L} e_R) \, (\overline{e_L} e_R) \\
& + \ g_3 \, (\overline{\mu_R} \gamma^\mu e_R) \, (\overline{e_R} \gamma_\mu e_R) + g_4 \, (\overline{\mu_L} \gamma^\mu e_L) \, (\overline{e_L} \gamma_\mu e_L) \\
& + \ g_5 \, (\overline{\mu_R} \gamma^\mu e_R) \, (\overline{e_L} \gamma_\mu e_L) + g_6 \, (\overline{\mu_L} \gamma^\mu e_L) \, (\overline{e_R} \gamma_\mu e_R) \ + \ H.c. \Big]
\end{aligned} \tag{2.1}
$$

where the form factors $A_{R,L}$ describe tensor-type (dipole) couplings, which contribute to $\mu^+ \to e^+ e^- e^+$ primarily through higher-order photon penguin diagrams; the other terms describe tree-level contact interactions with $g_{1,2}$ describing scalar-type and g_{3-6} vector-type interactions.

The expected constraints on these effective operators have been studied in detail in, for example, [12]. Figure 1 (from [12]) shows the allowed regions in two planes, defined by Wilson coefficients C_{ee}^{VRR} (equivalent to g_3 in eq. 2.1), C_{ee}^{SLL} (equivalent to g_1 in eq. 2.1), and C_L^D (equivalent to A_R in eq. 2.1). It is worth noting that, for the purely leptonic contact-type interactions (Fig. 1a), Mu3e is perhaps unsurprisingly the most sensitive. The other channels ($\mu^+ \to e^+ \gamma$ and $\mu^- N \to e^- N$) are also "blind" to certain regions of the parameter space due to cancellations, while this is never the case for $\mu^+ \to e^+ e^- e^+$. When considering the dipole-type interaction (Fig. 1b), the different channels are more complementary. When considering the flavour dependnce in the contact-type interactions, the muon conversion experiments set more strungent limits than $\mu^+ \to e^+ e^- e^+$ or $\mu^+ \to e^+ \gamma$. The studies in [12] highlight the degeneracy between different terms in the effective Lagrangian in 2.1, and the need for inputs from all three muon decay channels in order to resolve such degeneracy in the event of any observation of a signal.

The general effective Lagrangian in Eq. 2.1 can also be used to study signal kinematics and provides an important input in the design of the Mu3e experiment. Two important considerations are the acceptance, defined as the fraction of $\mu^+ \to e^+ e^- e^+$ decays where all decay products have a transverse momentum p_T above some minimal value $p_{T,min}$; and the energy distribution of the highest energy decay product in $\mu^+ \to e^+ e^- e^+$ decays. Both distributions are shown in Fig. 2 (taken from [1]) and illustrate that maximising sensitivity requires the ability to reconstruct electrons from half the muon mass down to as low as possible in p_T.
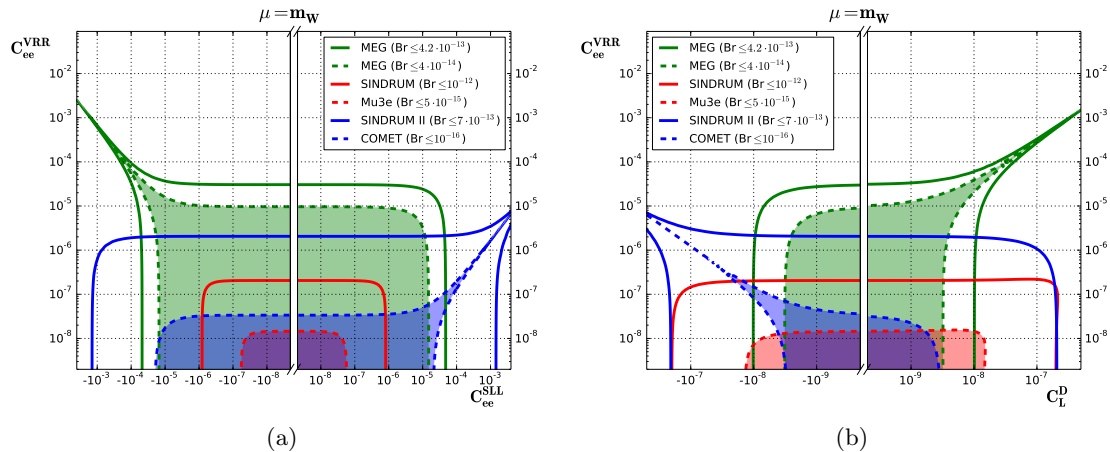
Figure 1. Allowed regions (given at the scale m_W) in the 1a C_{ee}^{VRR} - C_{ee}^{SLL} plane, and the 1b C_{ee}^{VRR} - C_L^D plane. Existing (solid lines) and projected (dashed lines) are shown for $\mu^+ \to e^+\gamma$ (green), $\mu^+ \to e^+e^-e^+$ (red) and $\mu^- N \to e^- N$ (blue). Figures from [12].
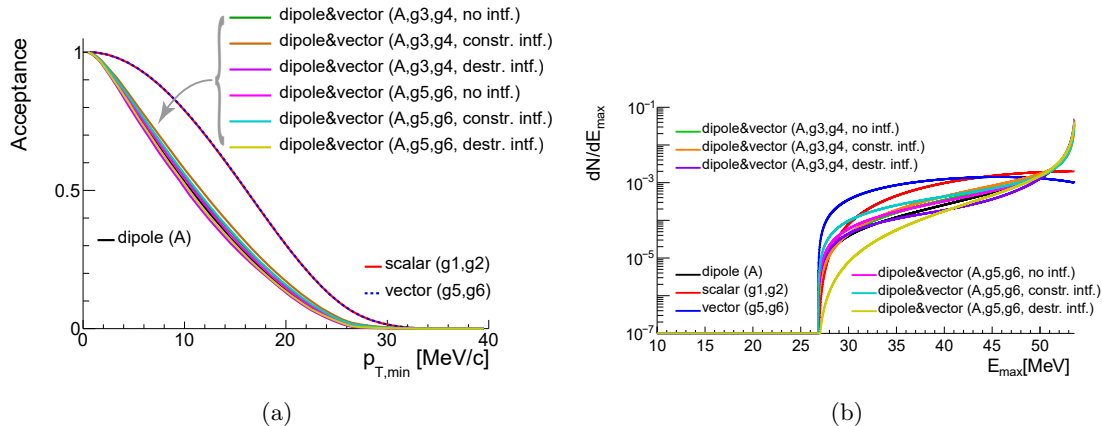

Figure 2. 2a the acceptance, defined as the fraction of $\mu^+ \to e^+e^-e^+$ decays where all decay products have p_T greater than $p_{T,min}$. 2b the energy distribution of the highest energy decay product in $\mu^+ \to e^+e^-e^+$ decays. Both are shown for the range of effective operators defined by 2.1. Figures from [1].

The other key consideration in the $\mu^+ \to e^+e^-e^+$ search is backgrounds, which fall into two categories: physics and combinatorics. The primary physics background is *internal conversion*: $\mu^+ \to e^+e^-e^+\nu_e\overline{\nu}_\mu$, which can be separated from the signal by the presence of two neutrinos. Combinatorics arise from the coincidence of one or more standard Michel decays with an e^- arising primarily from Bhabha scattering or radiative decay ($\mu^+ \to \overline{\nu}_\mu e^+\nu_e\gamma$) with subsequent photon conversion in the material of the detector. The three tracks in such cases typically do not have a common origin, and are not coincident in time.

All backgrounds can be controlled using vertexing and kinematic requirements, selecting three tracks consistent with $e^+e^-e^+$ from a common origin, and with the reconstructed vertex momentum < 4 MeV and mass consistent with the muon mass (103 MeV< m_{eee} <

110 MeV). The combinatoric background can be further reduced by coincident timing requirements, with time resolutions below 100 ps required to obtain a two orders of magnitude reduction. These physics requirements drive the design of the Mu3e experiment, which combines an extremely low material budget tracking detector with scintillating fibres and tiles for timing measurements. The Phase-1 Mu3e design is briefly reviewed below, with full details in [1].

In order to obtain optimal momentum and vertexing resolution on low energy ($< m_\mu/2$) electrons, Mu3e consists of four layers of High-Voltage Monolithic Active Pixel Sensors (HV-MAPS) surrounding the muon stopping target. These sensors have a pixel size of $80 \times 80 \ \mu m^2$, and are thinned to 50 μm giving a thickness of $X/X_0 = 0.1\%$ per layer when including the full assembly. Between the second and third pixel layers, the scintillating fibre detector provides the first time measurement. The fibre detector consists of three layers of 250 μm diameter fibres, providing a time resolution of 250 ps with an overall thickness of $X/X_0 = 0.2\%$. The entire detector sits in a wide-bore (1 m diameter) superconducting solenoid magnet providing a 1 T field.

In this multiple-scattering dominated regime, optimal momentum resolution is obtained for tracks which "recurl" in the magnetic field and pass through the detector a second time. To increase the acceptance for such tracks, upstream and downstream *recurl stations*, consisting of two further layers of pixel sensors surrounding a layer of plastic scintillator tiles are installed. Individual tiles measure $6.3 \times 6.2 \times 5 \text{mm}^3$, and are mounted in seven modules of 416 tiles each to provide full azimuthal coverage in each recurl station. The size of the tiles is chosen to provide improved time resolution (< 50 ps) compared to the fibre detector, with a thickness which ensures high ($> 99\%$) efficiency. The additional scattering in the tiles is not relevant, as only the pixel hits before reaching the tiles are used in track fitting. Figure 3 shows the layout of the Phase-1 Mu3e detector.
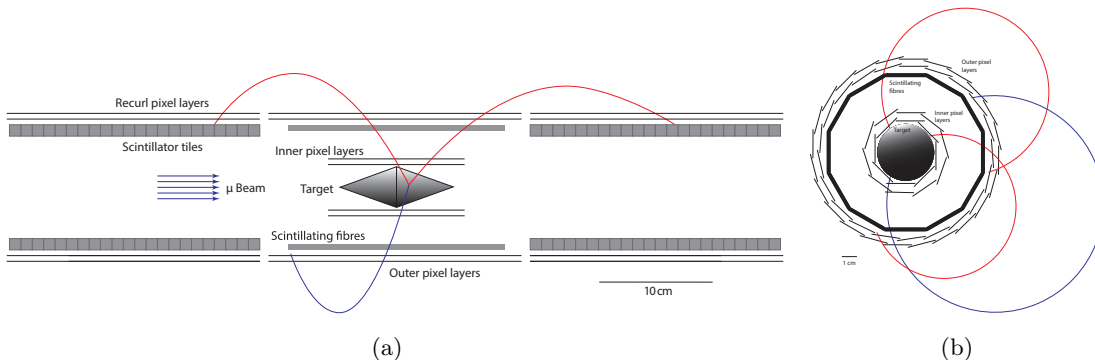

Figure 3. The layout of the Phase-1 Mu3e detector. Figures from [1].

The high rate of coincidences means that simply triggering on three coincident tracks does not provide a sufficient reduction in data rate to storage. Instead, Mu3e will operate with a continuous, triggerless readout, with a fast online track reconstruction used to select events containing three tracks consistent with a common vertex. The online reconstruction is based on time-slices ("frames") of the full detector readout, with 4-hit tracks

reconstructed in each frame on a GPU farm. The full offline tracking and signal selection, based on longer recurling (6 or 8 hit) tracks to optimise resolution, is then carried out on the stored frames. Figure 4a shows the expected vertex mass distribution based on the full offline selection. Figure 4b shows the expected evolution of sensitivity with running time; existing limits will be superseded within days, and the target sensitivity reached with around 400 days of data taking with a muon stopping rate of 1×10^8 s^{-1}.

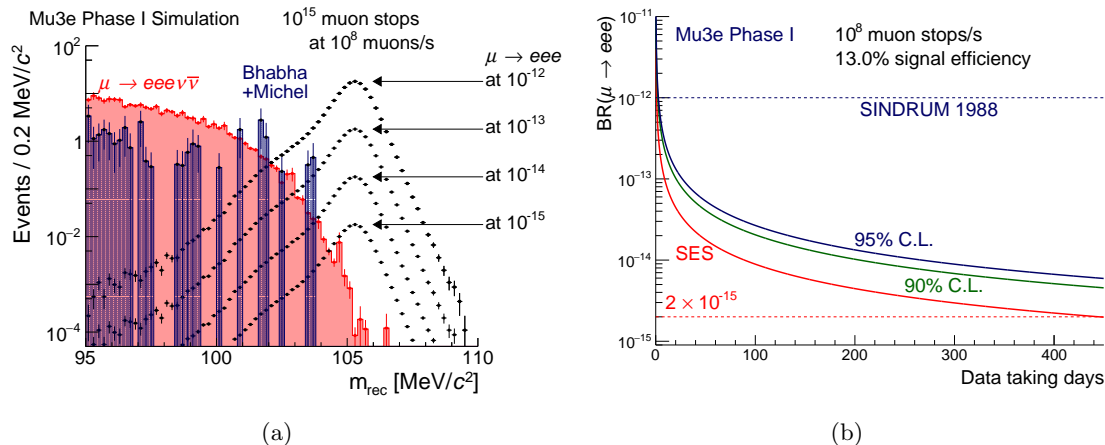(a)   (b)

Figure 4. 4a Simulation of the reconstructed vertex mass showing backgrounds and possible signal contributions. 4b the evolution of the Mu3e Phase 1 signal sensitivity with time. Figures from [1]

.

Mu3e Phase-2

To reach the final target sensitivity of 10^{-16} on the branching fraction for $\mu^+ \to e^+ e^- e^+$, a higher rate of muon stops is required. The High Intensity Muon Beam (HiMB) currently under study at PSI would deliver a stopping rate of 2×10^9 s^{-1}, but is not expected to be available before 2028. In order to deal with this higher stopping rate and resultant higher occupancy and rate of coincident backgrounds, upgrades to the Mu3e timing detectors are necessary, as well as possible improvements to the pixel sensors to improve time resolution, and extensions to the detector stations to increase the acceptance. Such upgrades are currently under study.

3   The search for $\mu^+ \to e^+ X$

In addition to searches for $\mu^+ \to e^+ e^- e^+$ decays, Mu3e can also investigate lepton-flavor-violating decays of the type $\mu^+ \to e^+ X$, where X denotes a neutral light particle that escapes the experiment undetected. An example for such a particle is the familon which arises as a pseudo-Goldstone boson from an additional broken flavour symmetry [13]. The current strongest limits on the branching ratio of $\mu^+ \to e^+ X$ are set by the experiment by Jodidio et al. at TRIUMF [14] for massless X with $\mathcal{B}(\mu^+ \to e^+ X) < 2.6 \times 10^{-6}$ at 90% CL, as well as the TWIST experiment [15] for $13\,\text{MeV} < m_X < 80\,\text{MeV}$ with $\mathcal{B}(\mu^+ \to e^+ X) < 9 \times 10^{-6}$ at 90% CL on average.

(a) Simulated background events.

(b) Simulated $\mu^+ \to e^+ X$ signal events with $m_X = 60\,\text{MeV}$.

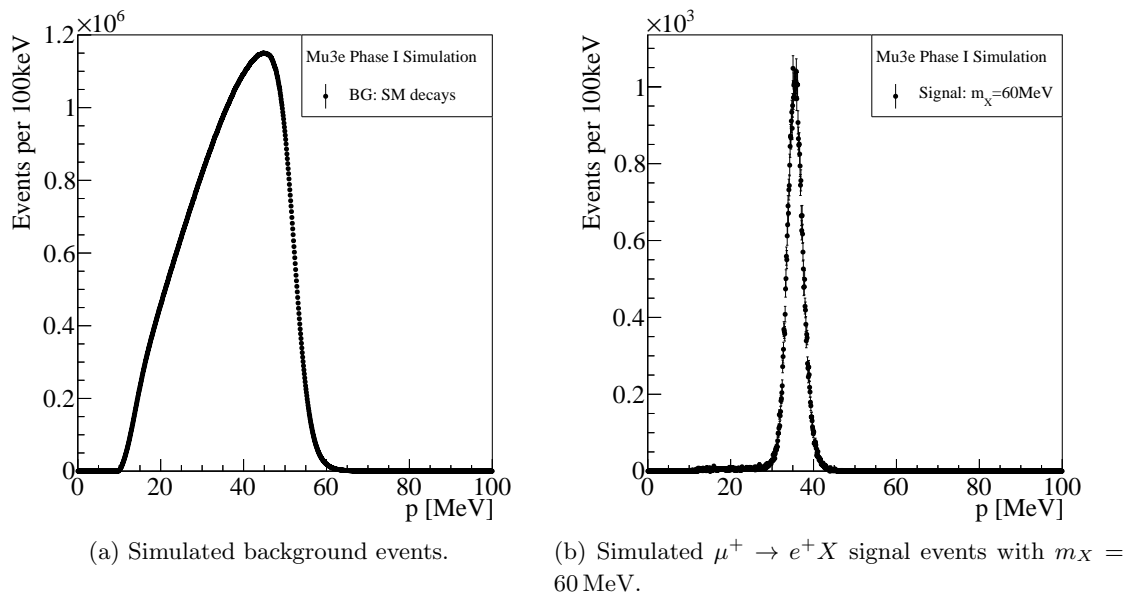**Figure 5**. Spectra of the reconstructed positron momentum of simulated background events from Standard Model muon decays (background) and $\mu^+ \to e^+ X$ events with $m_X = 60\,\text{MeV}$. The tracks are reconstructed from 4 hits in the central detector like it is done on the GPU filter farm.

The characteristic signature of $\mu^+ \to e^+ X$ decays is a mono-energetic positron whose energy is determined by the mass m_X of the undetected particle X. These positrons would appear as a narrow peak on top of the smooth momentum spectrum of positrons from Standard Model muon decays. In contrast to the $\mu^+ \to e^+ e^- e^+$ search, the final state contains only a single positron and would thus not pass event filtering on the online GPU farm. Therefore, a dedicated search strategy is required, and the analysis is performed on histograms which are filled with track fit information as part of the online track reconstruction. Since the full track reconstruction of all tracks in every event frame is performed online, histograms of the total momentum as well as the azimuthal and polar angle of the decay electrons and positrons can be recorded. This unprecedented dataset of the order of 10^{15} μ^+ decays allows not only for $\mu^+ \to e^+ X$ searches but also for studies of Standard Model μ^+ decays. As a drawback of this approach, event-by-event information is lost and the offline reprocessing of track reconstruction is not possible so that the optimum momentum resolution of recurling tracks cannot be achieved.

The acceptance of the Mu3e detector determines the mass reach of the search. With a minimum $p_T(e)$ of about $10\,\text{MeV}$ for the positron to be reconstructed, m_X of at most $95\,\text{MeV}$ can be studied. It is worth noting that complementary experiments sensitive to higher m_X up to the muon mass are currently being discussed [16]. Low m_X might be out of reach as well, as the characteristic edge of the momentum spectrum of Michel decays $\mu^+ \to e^+ \nu \overline{\nu}$ is currently used for calibration. Alternative calibration methods based on Bhabha and Mott scattering are under investigation.

The sensitivity in Phase 1 of the Mu3e experiment is estimated in toy Monte Carlo
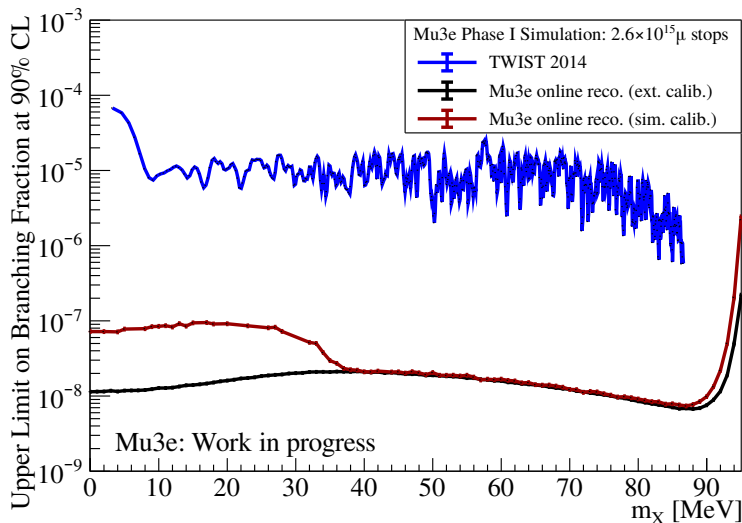
Figure 6. Expected limits on the branching fraction $\mathcal{B}(\mu^+ \to e^+X)$ at $90\,\%$ CL for various masses m_X. The momentum calibration is either obtained from the same spectrum leaving out a window around the $\mu^+ \to e^+X$ signal (red line), or from another process such as Bhabha or Mott scattering (black line). The current strongest observed limits by the TWIST experiment [15] are shown for comparison (blue line). TWIST results by courtesy of R. Bayes.

studies based on simulated momentum spectra. Signal and background events are simulated with the Geant4-based simulation of the Mu3e experiment. Standard Model muon decays form the background dominated by the Michel decay $\mu^+ \to e^+\nu\overline{\nu}$. Additional effects like tracks from Bhabha scattering or tracks which recurl multiple times are also considered as background contributions. Signal decays are simulated as two-body decays.

The tracks are reconstructed from 4 hits as in the online track reconstruction. The reconstructed momentum spectra for background events and $\mu^+ \to e^+X$ signal events with an exemplary mass of $m_X = 60\,\text{MeV}$ are shown in Figure 5.

In Figure 6, the expected sensitivity of the Phase 1 Mu3e experiment is shown for two different calibration approaches. In the first scenario, the calibration is derived from the Michel spectrum. In this approach, a momentum window around the the expected $\mu^+ \to e^+X$ signal is left out during the calibration step. In the second scenario, it is assumed that the calibration is derived in an alternative way for example with Bhabha or Mott scattering events. In the first scenario, the sensitivity is deteriorated when the left out momentum window covers the Michel edge, i.e. at low m_X.

In the first phase of the Mu3e experiment, $\mu^+ \to e^+X$ decays with branching ratios in the order of 10^{-8} can be tested, an improvement in sensitivity by a factor of around 600 with respect to the results by the TWIST experiment [15]. In addition to increased statistics in Phase 2, this search could further profit from improvements in momentum resolution. The feasibility of online reconstruction of long 6 or 8 hit tracks in view of the Phase 2 upgrade is currently being investigated.

4 The search for $\mu^+ \rightarrow e^+ +$ long-lived particles

The Mu3e dataset will allow searches for muon decays to light pseudoscalar particles that are long-lived and decay within the first silicon layer. An exploratory analysis documented in Ref. [17] has shown that such a final state in Mu3e has competitive sensitivity to other experiments. This analysis, however, has not used a detailed simulation of the Mu3e detector. In this section, this study is repeated using the latest Mu3e detector simulation and realistic track and vertex selection criteria.

In Ref. [17] axion-like particles, a, are considered with couplings to the SM leptons ℓ_α with $\alpha = e, \mu, \tau$ parameterized as:

$$\mathcal{L}_a = \frac{1}{\Lambda} \, \partial_\mu a \, \bar{\ell}_\alpha \gamma^\mu (g^V_{\alpha\beta} + g^A_{\alpha\beta} \gamma^5) \ell_\beta \, , \tag{4.1}$$

where Λ is an effective energy scale and g^V, g^A are the current structure matrices. From this interaction term, the decay width of the muon decay $\mu \rightarrow ea$ and, hence, its branching ratio, is found to be proportional to $m^3_\mu/(16\pi\Lambda^2_{\mu e})$ where $\Lambda_{e\mu} = \Lambda/\sqrt{(g^V_{e\mu})^2 + (g^A_{e\mu})^2}$ with the proportionality factor being a function of m_a and m_e under the approximation that $m_\mu \gg m_e$. The current structure matrices are assumed that they are such that the axion-like particle a decays only to ee with a lifetime that is calculated from the width $\Gamma(a \rightarrow ee)$ and is found to be proportional to the particle masses and $\Lambda_{ee} = \Lambda/g^A_{ee}$. Therefore, the free parameters for this model are (i) the mass of the axion-like particle m_a, (ii) $\Lambda_{e\mu}$ that controls the branching ratio of the decay, and (iii) Λ_{ee} that controls the lifetime of a and hence the location of its decay vertex inside the detector.

Muon decays to axion-like particles a are generated using[1] MadGraph5_aMC@NLO [18] and the resulting decay products are reconstructed using the Mu3e detector simulation. The same selection criteria for tracks and vertices are used as in the standard $\mu \rightarrow eee$ signal search, described in Ref. [1].

In this particular decay, the muon is assumed to stop on the target and to decay back-to-back to an electron and an axion-like particle a. The a particle will have a given boost and will decay depending on the assumed lifetime to two electrons. Due to the topology of the decay, the electron from the muon decay has a track that, if extrapolated, will meet the a particle's decay vertex. Therefore, for as long as there is no requirement for the reconstructed vertices to be close to the target surface, the Mu3e vertex reconstruction should be very efficient. The distance of the reconstructed vertex of the eee system from the actual a particle decay vertex for long tracks selected for this analysis is shown in Fig. 7a. This distribution is compatible with the vertex resolution performance for $\mu \rightarrow eee$ decays. The efficiency on signal of various m_a and lifetime values, as well as the efficiency for $\mu \rightarrow eee$ decays for comparison, is shown in Fig. 7b. No requirement on the distance of the vertices from the target is applied for these results.

The efficiencies shown in Fig. 7b are interpreted in the m_a–Λ_{ee} plane for different values of $\Lambda_{e\mu}$ assuming the Mu3e Phase 1 expected muon decays on target as a 90% confidence
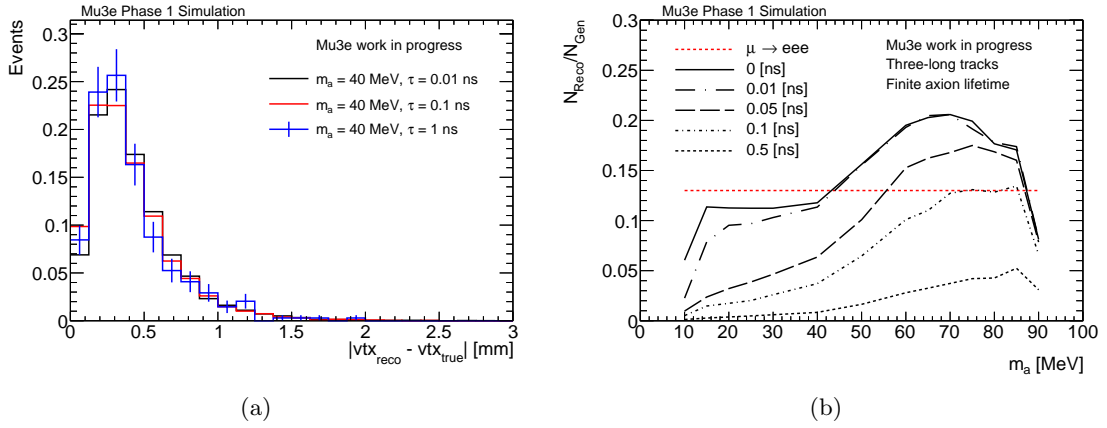

Figure 7. The distance between the reconstructed vertex of the $e^+e^+e^-$ system using the standard Mu3e experiment vertex reconstruction algorithm and the true vertex of the axion-like particle is shown in (a). This is for an axion-like particle of mass 40 MeV and lifetimes of 0.01 ns, 0.1 ns and 1 ns. The efficiency of the standard Mu3e experiment signal selection for axion-like particle masses in the range 10–90 MeV and for a range of lifetimes is shown in (b).
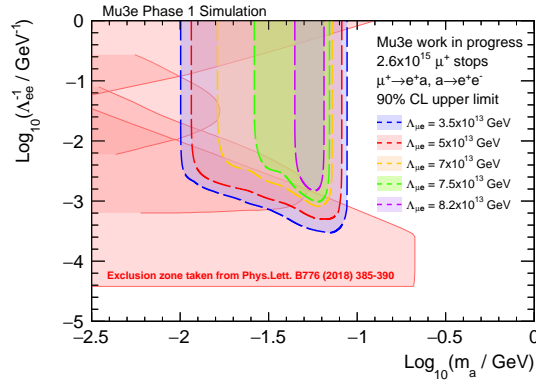

Figure 8. Upper limits in the two dimensional parameter space of the simple axion-like particle model discussed in the text.

level upper limit assuming no signal is found in a zero background experiment. This is shown in Fig. 4. On the same figure, exclusions from beam dump experiments and electron $g - 2$ reproduced from Ref. [17] are also shown. The whole available region of the m_a–Λ_{ee} parameter space between the existing constraints and the muon mass kinematic cutoff is excluded for $\Lambda_{e\mu} < 5 \times 10^{13}$ GeV. To reduce combinatoric backgrounds, a requirement on the distance between the vertex and target my be required. The impact of a ealistic value of 3 mm (suggested in Ref. [19]) has been studied and the outcome is that such a requirement has a small effect on the sensitivity and does not impair the sensitivity of the analysis to the axion parameter space.

5 The search for e^+e^--resonances in $\mu^+ \to e^+e^-e^+\nu_e\overline{\nu}_\mu$

In addition to $\mu^+ \to e^+e^-e^+$ searches and searches for long-lived particles, the dataset that will be recorded by the Mu3e experiment also allows for searches for resonances in $\mu^+ \to e^+e^-e^+\nu_e\overline{\nu}_\mu$. One example that has been further studied are dark photon A$'$ decays into e^+e^- pairs.

The dark photon is the messenger of a potential vector portal to the dark sector. It interacts with Standard Model particles via kinetic mixing with the photon and Z boson, i.e. via coupling to the electro-magnetic current. If the dark photon is light enough, it can be radiated in muon decays: $\mu^+ \to \text{A}'e^+\nu_e\overline{\nu}_\mu$.

In the following, the Lagrangian from [20] is used with the parameter ϵ determining the strength of the kinetic mixing. In this study, the sensitivity of the Mu3e experiment to promptly decaying dark photons $\text{A}' \to e^+e^-$ emitted in muon decays is estimated with a simplified detector simulation and without considering background from Bhabha scattering events. In the study presented in the following, the full Mu3e detector simulation and event reconstruction are used.

Signal events are generated with MadGraph5_aMC@NLO 2.4.3 [18] up to dark photon masses of $m_{\text{A}'} = 80\,\text{MeV}$. At larger masses, the parameter space in reach of Mu3e is already excluded by existing experimental limits. The simulated dark photons decay promptly to e^+e^- so that the same track and vertex reconstruction as for the $\mu^+ \to e^+e^-e^+$ search can be employed.

The background is dominated by the rare muon decay $\mu^+ \to e^+e^-e^+\nu_e\overline{\nu}_\mu$. As additional background sources, accidental combinations of Bhabha scattering events with Michel decays are considered which contribute on average by a factor of 800 less than the rare muon decay. Further types of accidental background are even less likely and therefore not considered in this study.

Spectra of the reconstructed invariant e^+e^--mass m_{ee} for background and signal are shown in Figure 9. The signal distribution features a narrow peak on top of a broader distribution which stems from e^+e^--combination of the positron from the muon decay and the electron from the A$'$ decay. This contribution can be reduced by selecting the e^+e^--combination with the lower m_{ee} for lighter A$'$, and the combination with the higher m_{ee} for heavier A$'$. The optimum transition point lies around $45\,\text{MeV}$.

The sensitivity to prompt dark photon decays in muon decays in the Phase 1 Mu3e experiment is estimated with toy Monte Carlo studies. At low $m_{\text{A}'}$, branching fractions of 5×10^{-9} at 90% CL can be investigated, while at higher $m_{\text{A}'}$, branching fraction of 3×10^{-12} at 90% CL can be reached (see Figure 10a). The expected limits on the branching fraction are translated into limits on the kinetic mixing parameter ϵ. The reach in the $\epsilon - m_{\text{A}'}$ parameter of the Phase 1 Mu3e experiment is shown alongside observed limits is shown in Figure 10b.
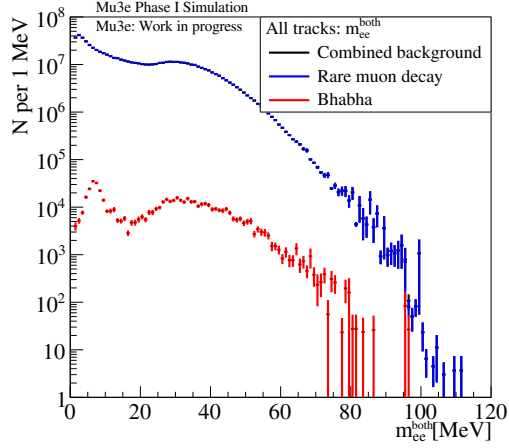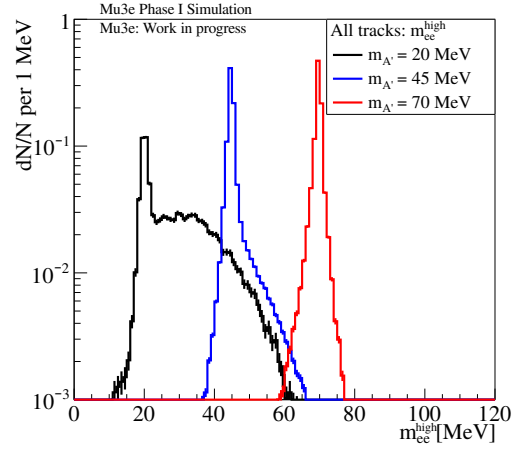
(a) Simulated background events. Both combinations of e^+e^- are considered.
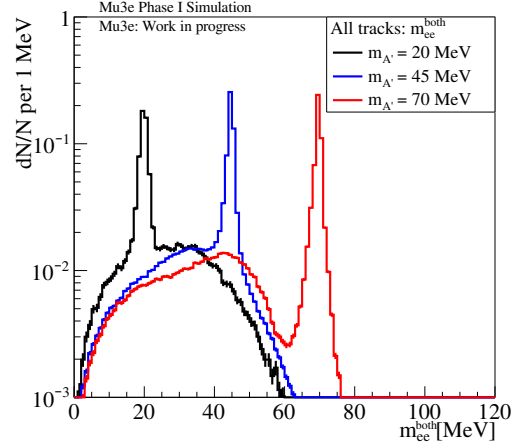
(b) Simulated A$'$ signal events. Both combinations of e^+e^- are considered.
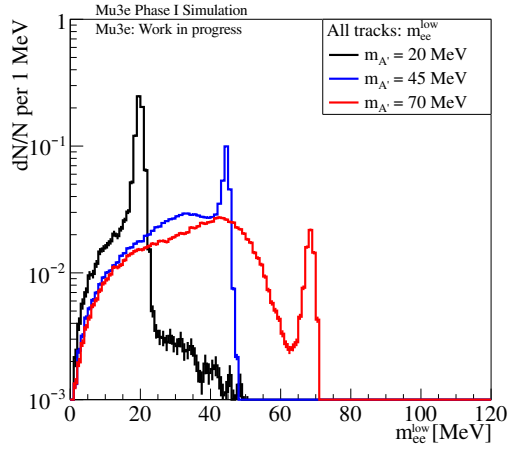
(c) Simulated A$'$ events. The e^+e^--combination with the lower invariant mass is shown.
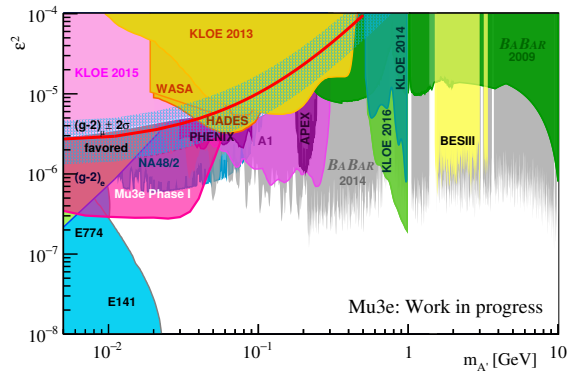
(d) Simulated A$'$ signal events. The e^+e^--combination with the higher invariant mass is shown.

Figure 9. Spectra of the reconstructed invariant mass m_{ee} of simulated background and dark photon signal events with $m_{A'} = 20\,\mathrm{MeV}, 45\,\mathrm{MeV}$ and $70\,\mathrm{MeV}$.
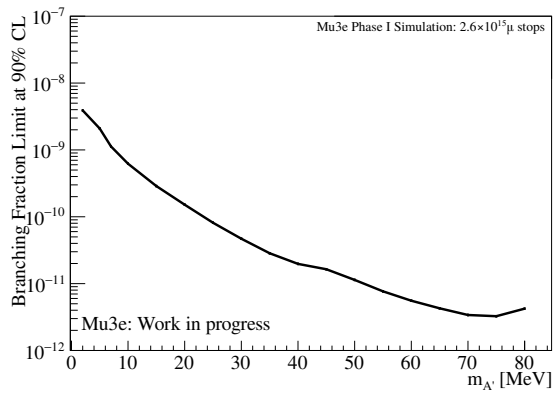
(a) Expected limits on the branching fraction at 90% CL.

(b) Expected limits on the kinetic mixing parameter ϵ at 90%CL. Adapted from [21].

Figure 10. Expected sensitivity to prompt dark photon decays in $\mu^+ \to e^+e^-e^+\nu_e\overline{\nu}_\mu$ in the first phase of the Mu3e experiment.

6 Conclusion

The Mu3e experiment will search for the lepton-number-violating decay $\mu^+ \to e^+ e^- e^+$. Using a two-phase approach and innovative design, it will extend the sensitivity to the branching ratio for this process to 10^{-16}, four orders of magnitude beyond current limits. In the context of the global programme covering $\mu^+ \to e^+ e^- e^+$, $\mu^+ \to e^+ \gamma$ and $\mu^- N \to e^- N$, Mu3e provides unique and complementary sensitivity to flavour-violating new physics.

The Mu3e experimental design also allows the search for a range of other processes, including dark photons, axion-like particles and long-lived particles. In each case, Mu3e can extend existing sensitivities in the accessible range of parameter space for such models.

Acknowledgements

References

[1] Mu3e collaboration, K. Arndt et al., *Technical design of the phase I Mu3e experiment*, *Nucl. Instrum. Meth. A* **1014** (2021) 165679, [2009.11690].

[2] MEG collaboration, A. M. Baldini et al., *Search for the lepton flavour violating decay* $\mu^+ \to e^+ \gamma$ *with the full dataset of the MEG experiment*, *Eur. Phys. J. C* **76** (2016) 434, [1605.05081].

[3] MEG II collaboration, A. M. Baldini et al., *The design of the MEG II experiment*, *Eur. Phys. J. C* **78** (2018) 380, [1801.04688].

[4] Mu2e collaboration, L. Bartoszek et al., *Mu2e Technical Design Report*, 1501.05241.

[5] COMET collaboration, R. Abramishvili et al., *COMET Phase-I Technical Design Report*, *PTEP* **2020** (2020) 033C01, [1812.09018].

[6] N. Teshima, *Status of the DeeMe Experiment, an Experimental Search for μ-e Conversion at J-PARC MLF*, *PoS* **NuFact2019** (2020) 082, [1911.07143].

[7] S. Petcov, *The processes* $\mu \to e\gamma$, $\mu \to e^- e^- e^+$, *neutrino' → neutrino* γ *in the weinberg-salam model with neutrino mixing*, *Soviet Journal of Nuclear Physics* **25** (1977) 340.

[8] P. Blackstone, M. Fael and E. Passemar, $\tau \to \mu\mu\mu$ *at a rate of one out of* 10^{14} *tau decays?*, *Eur. Phys. J. C* **80** (2020) 506, [1912.09862].

[9] L. Calibbi and G. Signorelli, *Charged Lepton Flavour Violation: An Experimental and Theoretical Introduction*, *Riv. Nuovo Cim.* **41** (2018) 71–174, [1709.00294].

[10] SINDRUM collaboration, U. Bellgardt et al., *Search for the Decay $\mu^+ \to e^+e^+e^-$*, *Nucl. Phys. B* **299** (1988) 1–6.

[11] Y. Kuno and Y. Okada, *Muon decay and physics beyond the standard model*, *Rev. Mod. Phys.* **73** (2001) 151–202, [`hep-ph/9909265`].

[12] A. Crivellin, S. Davidson, G. M. Pruna and A. Signer, *Renormalisation-group improved analysis of $\mu \to e$ processes in a systematic effective-field-theory approach*, *JHEP* **05** (2017) 117, [`1702.03020`].

[13] F. Wilczek, *Axions and Family Symmetry Breaking*, *Phys. Rev. Lett.* **49** (1982) 1549–1552.

[14] A. Jodidio et al., *Search for Right-Handed Currents in Muon Decay*, *Phys. Rev.* **D34** (1986) 1967.

[15] TWIST collaboration, R. Bayes et al., *Search for two body muon decay signals*, *Phys. Rev.* **D91** (2015) 052020, [`1409.0638`].

[16] D. Koltick, S. Huang, F. Bergin, J. Chen and H. Cao, *Muχe – A Search for Familons in Muon Decay Using HPGe Detectors*, 10, 2021, `2110.02164`.

[17] J. Heeck and W. Rodejohann, *Lepton flavor violation with displaced vertices*, *Phys. Lett. B* **776** (2018) 385–390, [`1710.02062`].

[18] J. Alwall, R. Frederix, S. Frixione, V. Hirschi, F. Maltoni, O. Mattelaer et al., *The automated computation of tree-level and next-to-leading order differential cross sections, and their matching to parton shower simulations*, *JHEP* **07** (2014) 079, [`1405.0301`].

[19] A.-K. Perrevoort, *Sensitivity Studies on New Physics in the Mu3e Experiment and Development of Firmware for the Front-End of the Mu3e Pixel Detector*, Ph.D. thesis, U. Heidelberg (main), 2018. 10.11588/heidok.00024585.

[20] B. Echenard, R. Essig and Y.-M. Zhong, *Projections for Dark Photon Searches at Mu3e*, *JHEP* **01** (2015) 113, [`1411.1770`].

[21] BESIII collaboration, M. Ablikim et al., *Dark Photon Search in the Mass Range Between 1.5 and 3.4 GeV/c^2*, *Phys. Lett.* **B774** (2017) 252–257, [`1705.04265`].